Accepted Manuscript

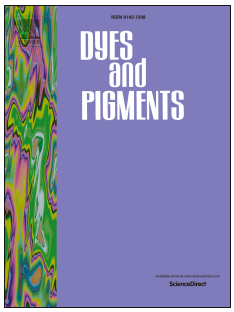

Neodymium doped yttrium aluminate synthesis and optical properties – A blue light emitting nanophosphor and its use in advanced forensic analysis

G.P. Darshan, H.B. Premkumar, H. Nagabhushana, S.C. Sharma, B. Daruka Prasad, S.C. Prashanth

PII: S0143-7208(16)30281-9

DOI: 10.1016/j.dyepig.2016.06.029

Reference: DYPI 5313

To appear in: *Dyes and Pigments*

Received Date: 12 March 2016

Revised Date: 12 June 2016

Accepted Date: 20 June 2016

Please cite this article as: Darshan GP, Premkumar HB, Nagabhushana H, Sharma SC, Prasad BD, Prashanth SC, Neodymium doped yttrium aluminate synthesis and optical properties – A blue light emitting nanophosphor and its use in advanced forensic analysis, *Dyes and Pigments* (2016), doi: 10.1016/j.dyepig.2016.06.029.

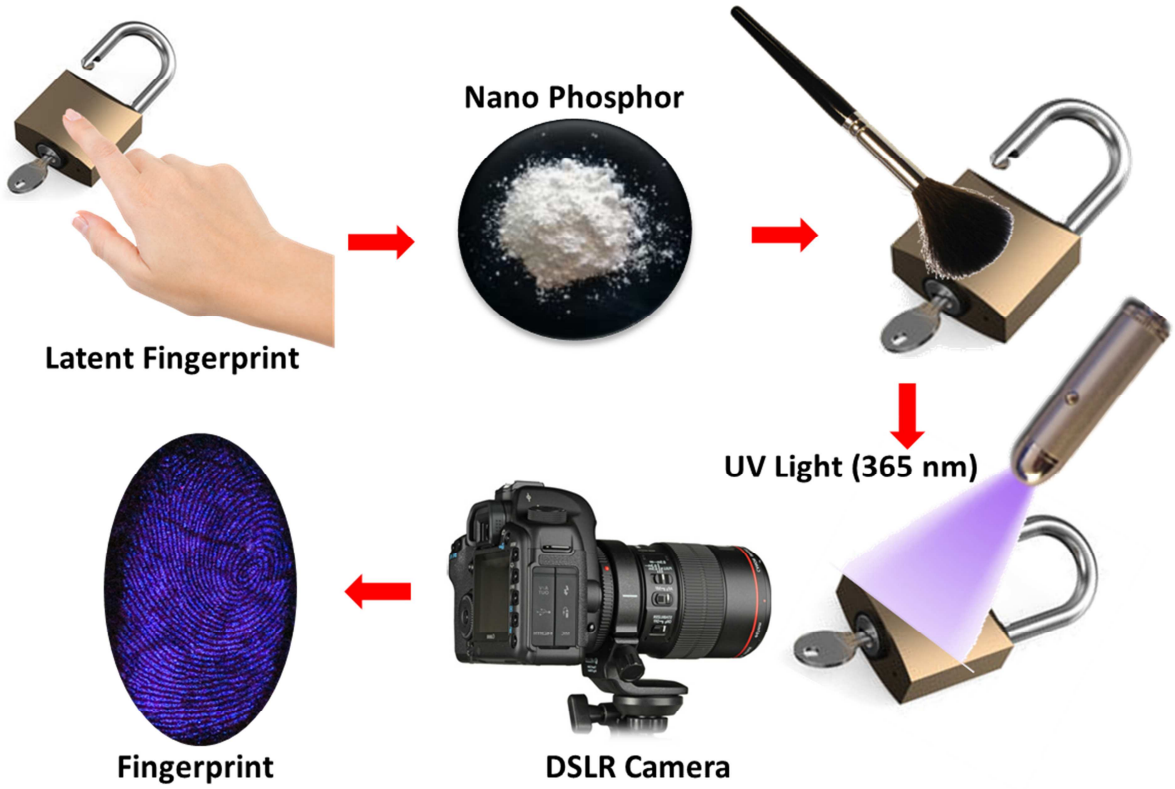

Neodymium doped yttrium aluminate synthesis and optical properties – A Blue light emitting nanophosphor and its use in advanced forensic analysis

G.P Darshan[1, 2], H. B Premkumar[3,*], H. Nagabhushana[4,*], S.C Sharma[5], B. Daruka Prasad[6], S. C Prashanth[7]

[1]Department of Physics, Acharya Institute of Graduate Studies, Bangalore 560 107, India
[2]Research and Development Center, Bharathiar University, Coimbatore 641046, India
[3]Department of Physics, Dayananda Sagar Academy of Technology and Management, Bangalore 560082, India
[4]Prof. CNR Rao Center for Advanced Materials, Tumkur University, Tumkur 572 103, India
[5]Dayananda Sagar University, Shavige Malleshwara Hills, Bangalore- 560078, India
[6]Department of Physics, BMS Institute of Technology and Management, VTU-affiliated, Bangalore 560 064, India
[7]Department of Science, East West Institute of Technology, Bangalore 560 091, India

* Corresponding authors. Tel.: +91-9880433880, E-mail: premhb@gmail.com (H B Premkumar) +91- 9945954010, E-mail addresses: bhushanvlc@gmail.com (H. Nagabhushana)

Abstract

A series of neodymium ions activated yttrium aluminate nanophosphors of various concentrations were synthesized by solution combustion method using oxalyl dihydrazide as a fuel. The crystal structure, optical energy gap, luminescent properties and Judd-Ofelt analysis were carried out. The use of the phosphor in revealing / enhancing the fingerprints quality was investigated in detail. The powder X-ray diffraction results confirmed the orthorhombic phase for the prepared samples. From diffuse reflectance spectra, estimated energy gap was found to be in range of 5.38-5.80 eV. The photoemission profile of $YAlO_3$: Nd^{3+} exhibit a blue emission upon 364 nm excitation. Further, the prepared materials were used for enhancing the quality of latent fingerprint technique. The present method was facile and robust for visualization of fingerprint with enhanced sensitivity, low glare light and high efficiency on various surfaces. The demonstrated results on facile detection of fingerprints virtually on any surfaces using $YAlO_3$:Nd^{3+} nanophosphors are versatile tool which hold great promise for practical applications on forensic sciences.

Keywords: Nanoparticles; Photoluminescence; Fingerprint; Forensic science; Solution combustion.

1. Introduction

Recently inorganic nanophosphors doped with various trivalent rare-earth (RE) ions have been an active area of research due to wide range of applications namely medical diagnostics, solid state lighting, display, optoelectronic devices, sensors, etc., [1-4]. It is well known that the aluminate based nanopowders (NPs) have been deployed in a variety of technologies such as plasma, field emission, and surface conduction electron displays [5-7]. Among aluminate based NPs, yttrium aluminate ($YAlO_3$) is most extensively produced laser gain host and as well as a substrate material for optical components. The Al_2O_3–Y_2O_3 system has three crystalline phases: $Y_3Al_5O_{12}$, $Y_4Al_2O_9$ and $YAlO_3$ of which the first two are stable and the latter is metastable. Among all the phases orthorhombic phase of $YAlO_3$ exhibit interesting properties such as high refractive index, better optical transparency, inert to toxic chemicals, fast scintillators, and ceramic pigments, etc., [8].

Aluminates are prepared by varies techniques namely solid state method, sol-gel, etc., among them solution combustion synthesis (SCS) is a versatile method due to its simple experimental set-up, molecular level of mixing, high degree of homogeneity, fast, cost effective, ultra-pure, large surface area etc. For the preparation of aluminates generally high temperature is required to obtain the desired phase as result the product is highly agglomerated and produce large surface defects. Due to this reasons the product is unfavorable to use in industry applications. However in SCS method, the product obtained is highly homogenous with less impurity and higher surface area [8, 9]. Further several experimental parameters can be designed in SCS method, namely F/O ratio, furnace temperature, etc. However to the best of our knowledge use of ODH fuel for the synthesis of $YAlO_3$ is limited.

DNA profiling is characteristics of individual DNA used in forensic labs to identify individuals. All unrelated individuals likely to be different with small set of DNA variations thereby being as unique to individuals as fingerprints. Even though the DNA profiling is most advanced, fingerprint (FP) recognition tool plays a major role in the recognition of individuals persons. Normally to recognize Latent FPs at crime scenes requires an enhancement for picturing and recognition. The practice of recognition to be used in each case depends on the characteristics of the FPs and the type of the surface on which they are found. Finding an easy and sensitive method to detect latent FPs effectively in forensic applications is essential [10].

Generally for FP revelation based on chemical categories can be classified into two types: (1) revelation technique that relies on non-covalent interactions such as dusting, gentian violet staining and small particle reagent. (2) revelation technique that involve chemical reactions such as ninhydrin, DFO (1, 8-diazafluoren-9-one), and silver nitrate. FP dusting is a simple technique that can be performed with almost any age group as it does not require specialized equipment except focused UV light, brush and uniform dusting powder.

Normally powdering method (PM) is preferred as a primary evidence for the FP detection at a crime scene. Generally, the PM method is categorized into regular, metallic and luminescent. PM method consists of a resinous polymer for adhesion and a colorant for contrast. Networked metals such as lead, gold and silver are used as powders for the detection of finger prints. This method is performed in proper ventilation and requires safety equipment's because of usage of toxic chemicals and their vapors. Some of the toxic chemical reagents used in this method of detection are listed in Table.1.

To overcome all the above limitations recently, luminescent based nano powders are used in latent FP detection. The size and shape of the NPs play an important role in strong bonding efficiency to the FP and these NPs adhere better than macro and micro particles [11]. Therefore, RE doped luminescent NPs have been explored as a potential technique in FP development has provoked the research community.

In the present work, synthesis, morphology and photoluminescence studies of Nd^{3+}:$YAlO_3$ NPs prepared via low temperature solution combustion route. The compounds were well characterized by PXRD, SEM, TEM, UV-Vis, PL, etc. Further an attempt has been made to apply the prepared nanopowders of $YAlO_3$:Nd^{3+} on various smooth surfaces namely aluminum foil, chocolate wrapping foil, mobile phone display screen and surface of a PET bottle. The prepared samples showed better usability in both latent fingermark detection and display device applications.

2. Experimental

2.1. Synthesis

All the chemicals used are of analytical grade and used without further purification. The stoichiometric ratios of yttrium nitrate [$Y(NO_3)_3.4H_2O$ (99.9%)], aluminum nitrate [$Al(NO_3)_3.9H_2O$ (99.9%)] and neodymium nitrate [$Nd(NO_3)_3.9H_2O$ (99.9%] are used as oxidizers and dopant to get a desired product of chemical formula $Y_xNd_{1-x}AlO_3$. The preparation process for ODH [$C_2H_6N_4O_2$] is explained elsewhere [9]. The oxidizer to fuel ratio is calculated based on oxidizers (O) and reducer (F) valences of the reactants, keeping O/F ratio as unity [12]. Aqueous solution containing all the above reactants are taken in 300 ml cylindrical petri dish and is placed in a preheated muffle furnace maintained at 400 ± 5 ^oC. The reaction mixture undergoes thermal dehydration and auto-ignites with the liberation of large gases [9]. The flame

propagates throughout the reaction mixture causing decomposition of the reactants and subsequent formation of the desired product. The obtained product is calcined at 1000 ºC for 3 h and used for further studies.

2.2. Characterization

Powder X-ray diffractometer (XRD, Shimadzu 7000) is used to measure phase purity and crystallinity of NPs using a Cuk_{α} (1.541Å) radiation. Scanning electron microscopy (SEM) (Hitachi table top, Model TM 3000) is used to analyze the surface morphology. Transmission electron microscopy (TEM) analysis is performed on a Hitachi H-8100 accelerating voltage up to 200 KV. Diffuse reflectance spectroscopy of the samples is analyzed by Perkin Elmer (35λ). The photoluminescence (PL) measurements are performed on a Jobin Yvon Spectroflourimeter Fluorolog-3 equipped with 450W Xenon lamp as an excitation source.

2.3. Relevance in FP development

Various smooth surface were chosen for the Latent FP experimental studies, includes non-porous surfaces such as aluminum foil, glass, and plastic etc. Before applying the FPs on few distinct surfaces, the donor hands were adequately washed and then pressed using medium pressure. The synthesized $YAlO_3:Nd^{3+}$NPs were used to develop ensuing latent FPs by cautiously applying powder on various surfaces and excess powder was removed by smooth brushing via a typical powder brush method. By using *in situ* with a Nikon D3100/ AF-S Nikkor 50 mm f/1.8G ED lens digital camera and a 365 nm UV light, images of developed FPs were photographed.

3. Results and discussion

The powder X-ray diffraction patterns (PXRD) of $YAlO_3:Nd^{3+}$ (1-11 mol %) NPs are shown in Fig. 1. All the PXRD peaks of the samples at (1 0 1), (1 1 1), (2 0 0), (1 2 1), (2 2 0) are well matched with JCPDS card No. 70–1677 of orthorhombic phase of $YAlO_3$ with small traces of

impurity peaks at 2θ = 29.50º and 30.82º corresponds to $Y_3Al_5O_{12}$ phase [8]. The PXRD lines are broadened due to the smaller crystallite size. The average crystallite size is determined using Scherrer's formula: $D = 0.9\lambda/\beta\cos\theta$, where D ; the average crystallite size, λ ;X-ray wavelength, θ ; the Bragg angle and β; the FWHM in radian. The average *D* values for all the doped samples are estimated and tabulated in Table 2.

According to the crystal field theory, the acceptable percentage difference in the ionic radii of doped and host ions must be less than 30 %. The acceptable percentage difference was estimated using the relation $D_r = (R_m - R_d)/R_m$ where R_m and R_d ; radii of host and dopant ions. The estimated value of D_r is found to be ~ 8.1 %. Due to close radius of both Nd^{3+} and Y^{3+} ions, it is assumed that dopant Nd^{3+}ions would replace the Y^{3+} ions in $YAlO_3$ host [14].

The SEM images of $YAlO_3$:Nd^{3+} (3 & 11 mol %) NPs are shown in Fig. 2(a, b). The product shows dumbbell in shape and crystallites are fused together to form agglomerated particles. TEM studies are carried out for the $YAlO_3$: Nd^{3+} (3 & 11mol %) samples (Fig. 3(a, b)). It is evident that the crystallites are in dumbbell with average size ~ 44 nm which is in well agreement with the values obtained in PXRD studies. The HRTEM (Fig. 3(c)) showed the well resolved lattice fringes with an estimated interplanar spacing of ~ 0.243 nm.

The diffused reflectance spectra (DRS) of Nd^{3+} doped $YAlO_3$ (1-11 mol %) NPs were as shown in Fig. S1. The spectra exhibits major peaks at ~ 275, 360, 529, 586, 680,742 and 806 nm due to the transitions of the 4f electrons of Nd^{3+} from the ground-state $^4I_{9/2}$to$^2F_{5/2}$, $^4D_{3/2}$+$^4D_{5/2}$+$^2I_{11/2,}$ $^2K_{13/2}$+$^4G_{7/2}$+$^4G_{9/2}$, $^4G_{5/2}$+$^2G_{7/2}$, $^4F_{7/2}$+$^4S_{3/2}$, $^4F_{5/2}$+$^2H_{9/2}$ and $^4F_{3/2}$ respectively [15, 16]. The intense light reflectance observed in UV region indicates that these materials are suitable in near-UV excited LED phosphors. The band gap energy (E_g) of all the samples are

determined by using Kubelka–Munk function. The plots of $[F(R_\infty)h\nu]^{1/2}$ versus photon energy $h\nu$ are shown in Fig. 4. The Kubelka–Munk function $F(R_\infty)$ and photon energy ($h\nu$) is calculated by using the relations [17, 18]:

$$F(R_\infty) = \frac{(1-R_\infty)^2}{2R_\infty} \quad \text{---------- (1)}$$

$$h\nu = \frac{1240}{\lambda} \quad \text{---------- (2)}$$

where R_∞; reflection coefficient of the sample, λ; the absorption wavelength. The measured band gap energies are tabulated in a table.1. The variation in the E_g are mainly attributed to the degree of structural order and disorder in the lattice [14].

Excitation spectra (Fig. 6 inset) from 300 to 460 nm specify the chance of effective excitation of Nd in the $O^{2-} \rightarrow Nd^{3+}$ charge transfer band (CT) maxima at 364 nm. The occurrence of this band is a result of O^{2-} ions in the structure. The energy of $O^{2-} \rightarrow Nd^{3+}$ CT could be estimated using the following equation given by Jørgensen [19].

$$E_{CT} = [\chi(L) - \chi(M)](3\times10^4) \quad \text{---------- (3)}$$

where E_{CT} denotes the position of the CT band in cm^{-1}, χ(L) and χ(M) are the opto-electronegativities of the O^{2-} and Nd^{3+} cations respectively. For χ(O) = 3.2 and $\chi(Nd^{3+})$ = 1.14 the calculated CT position should be 61,800 cm^{-1}. The measured position of CT bands in the excitation spectra of NPs is ~ 364 nm.

Upon 364 nm excitation (Fig. 5), the emission spectra exhibit a series of emission peaks at 495, 596, 613 and 645 nm corresponds to the transitions of $^2G_{9/2} \rightarrow {}^4I_{9/2}$, $^4G_{5/2}+{}^2G_{7/2} \rightarrow {}^4I_{9/2}$, $^2H_{11/2} \rightarrow {}^4I_{9/2}$ and $^4H_{9/2} \rightarrow {}^4I_{9/2}$ respectively [20]. Generally, the doping concentration has a significant effect on the NPs performance. The dependence of the blue emission (λ_{ex}=364 nm) on

the Nd^{3+} doping concentration (x) in the $YAlO_3:Nd^{3+}$ (1-11 mol %) NPs are shown in Fig.6. PL intensity increased with increase in Nd^{3+} concentration up to 3mol % and afterwards quenching starts. Initially, the PL intensity increases and then decreases due to smaller radius of Nd^{3+} as compared to Y^{3+} ions but at higher intensity the charge imbalance leads to cross relaxation and on radiative transitions causes concentration quenching [21].

The PL emission spectra of $YAlO_3:Nd^{3+}$ NPs are further used to calculate Judd–Ofelt (J-O) intensity parameters. From the emission spectra, the measured line strengths (S_{meas}) are determined by using Eq. (4). The J-O parameters Ω_2 and Ω_4 are obtained using least-squares fitting approach between the S_{meas} and the S_{cal}.

$$A_T = \frac{64\Pi^4 v^3 e^2}{3hc^3}\,\frac{1}{4\Pi\varepsilon_0}\,\chi \sum_{J=4,6}\Omega_J \left\langle {}^1D_0 \left| U^{(J)} \right| {}^3F_4 \right\rangle^2 \qquad \text{---------- (4)}$$

The J–O parameters (Ω_2 and Ω_4), $YAlO_3:Nd^{3+}$ (1-11 mol %) NPs are tabulated in Table 3. The value of Ω_2 varied with change of Nd^{3+} concentration shows Ω_2 is mainly sensitive to the ligand environment (short range effect) and Ω_4 is associated to the long-range effect. The important radiative properties such as transition probabilities (A_T), radiative lifetime (τ_R) and branching ratios (β_R) of the excited states of Nd^{3+} are calculated by using J–O parameters. The A_T for a transition $J \to J'$ is calculated from by an equation [22].

$$A_T(J \to J') = \frac{64\pi^4 v^3 e^2}{3h(2J+1)}\left[\frac{n(n^2+2)^2}{9} S_{ed} + n^3 S_{md}\right] \qquad \text{---------- (5)}$$

The radiative lifetime (τ_R) of an excited state is given by

$$\tau_R(J) = \frac{1}{\sum_{\psi J'} A_T(J \to J')} \qquad \text{---------- (6)}$$

β_R is a critical parameter for the laser designer because it characterizes the possibility of attaining stimulated emission on any specific transitions and also used to calculate the relative intensities of all emission transitions are given by

$$\beta_R(J, J') = \frac{A_T(J \rightarrow J')}{\sum_{J'} A_T(J \rightarrow J')} \quad \text{---------- (7)}$$

It is known that a transition having β_R of ≥ 0.50 can emit laser radiation more effectively. The measured β_R of 0.99 for Nd^{3+} doped $YAlO_3$ suggests its suitability for color displaying devices. All the obtained parameters for the Nd^{3+} ions in $YAlO_3$ host are listed in Table 3.

The CIE chromaticity diagram of $YAlO_3$:Nd^{3+} is shown in Fig.7 and the corresponding coordinates are tabulated in the Table 4. All the coordinates are well located within the blue region as a result the $YAlO_3$:Nd^{3+} NPs are promising materials for the production of artificial blue light which is similar to the natural blue light owing to its better spectral overlap in white LEDs and in solid state display applications. Further correlated color temperature (CCT) is also calculated by transforming the (x, y) coordinates of the light source to (U', V') by using following equations and by determining the temperature of the closest point of the Planckian locus to the light source on the (U', V') uniform chromaticity diagram (Fig.8) and Table 4 [23, 24].

$$U' = \frac{4x}{-2x + 12y + 3} \quad \text{---------- (8)}$$

$$V' = \frac{9y}{-2x + 12y + 3} \quad \text{---------- (9)}$$

The chemical composition of Latent FP residue

Firstly, understanding the chemical composition of FP residue is very crucial. Basically the chemical constituents are responsible for FP residue can be classified into two types based on originate from endogenous and exogenous sources. Whatever you have touched might transfer chemical residue on to your volar pads that could end up in your latent FPs. For example, cooking oil from that donut you ate for breakfast will probably be present in your FPs until you wash it off. Then residues from the soap you used to wash your hands may be a chemical constituent of your latent FPs. In fact, residue from personal care products is often found in latent FPs [25, 26].

Endogenous sources may be more predictable but more complexes. What we would call sweat and/or body oil comes from 4 different types of glands: eccrine, apocrine, apoeccrine, and sebaceous. Each gland secretes slightly different blend of chemical components. Generally, eccrine glands secrete classic sweat, an aqueous solution of electrolytes and hydrophilic compounds such as urea [27]. The other three glands secrete lipophilic fatty and waxy substances such as squalene and cholesterol [28, 29]. Constituents representing nearly all of the common chemical classifications can be detected in sweat and latent FPs: alcohols, phenols, aldehydes, ketones, esters, hydrocarbons, amines, amides, amino acids, and carboxylic acids [30−32]. In fact, a particular mix of chemicals may be as individualistic for a particular person as a FP. A thorough chemical analysis of FP residues may even reveal if the person habitually inhales or ingests certain chemical substances [33, 34]. In addition, it is quite likely, that the composition of latent FPs change as a person ages [35]. Latent FP residue composed primarily of lipids such as squalene, fatty acids, and cholesterol adheres to a large number of substances. The NPs must adhere to the FPs and not to the surface nearby the FPs is the requirement [36, 37].

Mechanism of latent FP development by using $YAlO_3$: Nd^{3+} NPs.

The strategy of latent-FP detection by using the Nd^{3+} doped $YAlO_3$ NPs under room conditions is illustrated in Fig. S2. The prepared powder is then applied to different surfaces by spreading, due sweat and fat in the finger print mark residue group the rapid physical adsorption of the $YAlO_3$: Nd^{3+} NPs onto the ridges produced on the substrate. Then, the substrate is excited in a UV chamber at 365 nm to visualize the latent fingermarks by a digital camera. The present method is convenient and easy to detect latent FP's without any complex or costly instrumentation compared to the reported literature [38 - 42].

FP detection using $YAlO_3$: Nd^{3+}NPs

The mechanisms of this strategy for FP detection is analyzed and the different nanomaterials used for develop latent FPs were tabulated in a Table 5. When a FP was deposited on the surface, 99% of the moisture quickly evaporates by leaving behind sodium chloride, potassium chloride and other inorganic materials and few traces of amino acids, organic components, polysaccharides and proteins.

Fig.9 shows luminescence images of FPs where the fine ridge details with better contrast can be observed which helps in easy identification of individuals. Because of this benefit, FPs developed with $YAlO_3$: Nd^{3+}NPs provided high quality images that show well resolved ridge patterns that meet the requirements for individual identification for forensic purposes.

The FP developed on the aluminum foil and yellow-colored chocolate wrapping sheet, there is an interference of background color with other regular/ordinary developing powder (Fig.10 a & b). Fig.10 (c & d) shows the FPs developed with $YAlO_3$: Nd^{3+} NPs on stainless steel knife edge and steel lock under UV light exposure clearly evident for the fine ridge details with

better contrast. Further, similar procedure is adopted to analyze the ridge patterns on the mobile phone display screen and PET bottle surfaces (Fig. 10 e & f).

FP patterns are studied for the different ageing periods to demonstrate the suitability of the prepared NPs. Fig. 11 shows the detective sensitivity gradually diminished with aging or stability of adherences of the dusting powder on the surface. It is apparent that the latent FPs aged up to one month clearly shows ridges, indicating that the sensitivity of the NPs.

The fresh FP deposited on glass plate exposed to different illuminations with a labeling of FPs under 254 nm, 365 nm (Fig. S4). The present results indicate that the optimized NPs reveal the whole FPs with better contrast. Further, the procedure is novel and rapid; an investigator needs to apply NPs immediately followed by imaging the FPs. In addition the developed FPs can be preserved for an extended time without losing their phosphorescence capability.

4. Conclusions

Dusting powder method was used for the detection of latent FP using $YAlO_3:Nd^{3+}$ NPs synthesized by SCS method. The average crystallite size was found to be in the range 30 - 32 nm. The crystallites were agglomerated with porous nature helps in better adhesion of NPs on various substrates. The E_g values estimated from DRS were found to be in the range 5.39 - 5.79 eV. The calculated CIE values correspond to blue color. The developed FP procedure was a facile with high sensitivity, low background, high efficiency and good adherence on porous/semi-porous/nonporous, multicolored surfaces which helps in developing latent FPs in forensic applications.

Acknowledgements

Author HBP thanks VGST, Government of Karnataka, India, (No. VGST/P-3/SMYSR/GRD-302/2013-14) for its help in carrying out this research work .The authors SCP, HPN and HBP thanks to VGST, Govt. of Karnataka, India, (No: VGST /CISEE /2012-13/282) for sanctioning the research project. The authors thanks to the DSU Management for providing the facility of high resolution camera to take the photographs of finger prints under various conditions.

References

1. F. Zhang, S.S. Wong, ACS Nano, 4 (2010) 99.
2. H. Wang, C.K. Lin, X.M. Liu, J. Lin, Appl. Phys. Lett., 87 (2005) 181907.
3. J. Heikenfeld, A.J. Steckl, IEEE Trans. Elect. Dev., 49 (2002) 1545.
4. N. Rakov, G.S. Maciel, Sens. Actu. B, 164 (2012) 96.
5. T. Aitasalo, J. Holsa, H. Junger, M. Lastusaari, J. Niittykoski, J. Alloys Compd. 341 (2002) 76.
6. V. Singh, J. Zhu, M. Bhide, V. Natarajan, Opt. Mater., 30 (2007) 446.
7. X. Xu, Y. Wang, Y. Li, Y. Gong, J. Appl. Phys., 105 (2009) 083502.
8. H.B. Premkumar, H. Nagabhushana, S.C. Sharma, S.C. Prashantha, H.P. Nagaswarupa , B.M. Nagabhushana, R.P.S. Chakradhar , J. Alloys Compd., 601 (2014) 75.
9. K.C. Patil, Chemistry of Nanocrystalline Oxide Materials, in: Combustion Synthesis, Properties and Applications, World Scientific, 2008.
10. M. Algarra, J. J. Jiménez, M. S. Miranda, B. B. Campos, R. M. Tost, E. R. Castellónb, J. C. G. E. Silva, Surf. Interface Anal., 45 (2013) 612.
11. M. Saif, J. Lumin., 135 (2013) 187.
12. S.T. Aruna, K.C. Patil, Nanostruct. Mater., 10 (1998) 955.
13. H.B. Premkumar, D.V. Sunitha, H. Nagabhushana, S.C. Sharma, B.M. Nagabhushana, J. L. Rao , K. Gupta , R.P.S. Chakradhar, J. Spectrochim. Acta A, 96 (2012) 154.
14. R. Naik, S.C. Prashantha, H. Nagabhushana, H.P. Nagaswarupa, K.S. Anantharaju, S.C. Sharma, B.M. Nagabhushana, H.B. Premkumar, K.M. Girish, J. Alloys Compd., 617 (2014) 69.

15. F. Peng, W. Liu, Q. Zhang, H. Yang, C. Shi, R. Mao, D. Sun, J. Luo, G. Sun, J. Crys. Gro., 406 (2014) 31.

16. L.K. Pan, Q. Sun Chang, C.M. Li, J. Phys. Chem. B, 108 (2004) 3404.

17. L. Wan, J.F. Li, J.Y. Feng, W. Sun, Z.Q. Mao, Mater. Sci. Eng. B, 139 (2007) 216.

18. J. Zhang, J. Xi, Z. Ji, J. Mater. Chem., 22 (2012) 17700.

19. C. K. Jørgensen, Electron Transfer Spectra, John Wiley & Sons, Inc., 1970.

20. Santosh K. Gupta, D. Chandrasekhar, R.M. Kadam, J. Mol. Struc., 1102 (2015) 141.

21. S. Som, A. K. Kunti, Vinod Kumar, Vijay Kumar, S. Dutta, M. Chowdhury, S. K. Sharma, J. J. Terblans, H. C. Swart, *J. Appl. Phys*. 115 (2014) 193101.

22. V. Venkataramu, P. Babu, C. K. Jayasankar, Th. Tr¨oster, W. Sievers, G. Wortmann, Opt. Mater., 29 (2007) 1429.

23. B. Judd, J. Deane, Opt. Soc. Am., 26 (1936) 421.

24. J. Schanda, M. Danyi, Color Res. Appl., 2 (1977) 161.

25. B. H. Baguley, R.E. Hipp, N.R. Morgan, S.L. Morgan, J. Chem. Educ., 84 (2007) 689.

26. M. Gallagher, C.J. Wysocki, J.J. Leyden, A.I. Spielman, X Sun, G. Preti, Br. J. Dermatol., 159 (2008) 780.

27. N. Liappis, S.D. Kelderbacher, K. Kesseler, P. Bantzer, Eur. J. Appl. Physiol., 42 (1979) 227.

28. J.N. Labows, G. Preti, E. Hoelzle, J. Leyden, A. Kligman, Steroids, 34 (1979) 249.

29. M. E. Stewart, D.T. Downing, J. Invest. Dermatol., 84 (1985) 501.

30. U.R. Bernier, D.L. Kline, D.R. Barnard, C.E. Schreck, R.A. Yost, Anal. Chem., 72 (2000) 747.

31. Z.M. Zhang, J.J. Cai, G.H. Ruan, G.K. Li, J. Chromatogr. B, 822 (2005) 244.

32. L. Ferguson, R. Bradshaw, R. W. Holme, M. Clench, S. Francese, Anal. Chem., 83 (2011) 5585.

33. P. Hazarika, D.A. Russell, Angew. Chem., Int. Ed., 51 (2012) 3524.

34. J. Brent Friesen, J. Chem. Educ., 92 (2015) 497.

35. A. Hemmila, J. McGill, D. Ritter, J. Forensic Sci., 53 (2008) 369.

36. G.S. Sodhi, J. Kaur, Forensic Sci. Int., 120 (2001)172.

37. M. Wang, M. Li, M. Yang, X. Zhang, A. Yu, Y. Zhu, P. Qiu, C. Mao, Nano Res., 8 (2015) 1800.

38. H. H. Xie, Q. Wen, H. Huang, T. Y. Sun, P. Li, Y. Li, X. F. Yu, Q. Q. Wang, RSC Adv., 5 (2015) 79525.

39. V. Sharma, A. Das, V. Kumar, O. M. Ntwaeaborwa, H. C. Swart, J Mater. Sci., 49 (2014) 2225.

40. M. J. Choi, K.E. McBean, P. H. R. Ng, Andrew M, M. Donagh, Philip J, M. C. Lennard, C. Roux, J Mater Sci., 43 (2008) 732.

41. Y. F. Wang, R. Q. Yang, Z. X. Shi, J. J. Liu, K. Zhao, Y. J. Wang, J. Saudi, Chem. Soci., 18 (2014) 13.

42. M. Saif, M. Sheb, A.I. Nabeel, R. Shokry, H. Hafez, A. Mbarek, K. Damak, R. Maalej, M. S. A. A. Mottaleb, Sens. Actuators B, 220 (2015) 162.

Table Captions:

Table.1: Hazards Associated with the some Reagents Used for the Chemical Revelation of FP Residues

Table.2: Estimated crystallite size and optical energy gap (E_g) values of $YAlO_3$:Nd^{3+} NPs.

Table.3: J-O intensity parameters (Ω_2, Ω_4), Emission peak wavelengths ($\lambda_p$in nm), radiative transition probability (A_T), calculated radiative lifetime(τ_{rad}) and branching ratio (β_R) of $YAlO_3$: Nd^{3+} compounds (λ_{ex} = 364 nm).

Table.4: The values of x, y coordinates and CCT (K) of $YAlO_3$: Nd^{3+}(1-11mol %) NPs.

Table.5: Different nanomaterials used for develop latent FPs by different authors.

Figure captions:

Fig.1. PXRD patterns of (1–11 mol %) Nd^{3+} doped $YAlO_3$NPs.

Fig.2. (a–b).SEM micrographs of $YAlO_3$:Nd^{3+} (3 and11 mol %) NPs.

Fig.3. (a–b).TEM micrographs of $YAlO_3$:Nd^{3+} (3 and11 mol %) NPs, (c) HRTEM image of $YAlO_3$:Nd^{3+} (5mol %).

Fig.4. Energy band gaps of (1–11 mol %) Nd^{3+} doped $YAlO_3$NPs.

Fig.5. Emission spectrum of $YAlO_3$:Nd^{3+} (1-11mol %) at λ_{exc}= 364 nm. Inset PL excitation spectra of $YAlO_3$:Nd^{3+} (3 mol %) NPs recorded at RT.

Fig.6. Effect of Nd^{3+}concentration on the 596 nm emission peaks in $YAlO_3$ NPs.

Fig.7. CIE diagram of $YAlO_3$:Nd^{3+} (1-11 mol %) NPs.

Fig.8. CCT diagram of $YAlO_3$: Nd^{3+} (1-11 mol%) NPs.

Fig.9. Latent FPs of different persons stained by $YAlO_3$:Nd^{3+}(3mol%)NPs and imaged on the surface of glass.

Fig.10. FPs developed with prepared NP on (a) aluminum foil (b) Chocolate wrapping foil (c) surface of knife handle (d) steel lock (e) mobile phone display screen and (f) surface of a PET bottle.

Fig.11. Latent FP aged on the surface of glass for various periods of time, stained by $YAlO_3$:Nd^{3+} (3 mol%) NP and finally detected by 365 nm UV light irradiation (a)1 day, (b) 10 days, (c) 30 days.

Table1. Hazards connected with the some reagents Used for the chemical revelation of FP residues

Sl.No	Chemicals	Hazards
1	Ninhydrin solution	Flammable. Harmful vapors. Skin and eye irritant.
2	DFO (1,8-diazafluoren-9-one) solution	Flammable. If inhaled it may be quit dangerous. May be absorbed through the skin. Respiratory and digestive region irritant. May cause skin andeye irritation.
3	Silver nitrate solution	Oxidizer. May be harmful if inhaled. Respiratory and digestive tract irritant. May cause skin and eye burns, argyria, a blue-gray discoloration of the skin, eyes, and mucous membranes.
4	Cyanoacrylate glue	Respiratory tract, eye and skin irritant. Bonds skin rapidly and strongly. May cause skin burns.
5	Iodine crystals	Oxidizer. May be harmful if inhaled, ingested, or contacted by skin or eyes. Respiratory irritation. May be corrosive to skin and eyes.
6	Gentian violet solution	May be absorbed through the skin. Respiratory, digestive, skin and eye area will getaggravation.

Table 2: Estimated crystallite size and optical energy gap (E_g) values of $YAlO_3:Nd^{3+}$ NPs.

$YAlO_3:Nd^{3+}$ (mol %)	**Crystallite size(nm) [D-S approach]**	**Crystallite size(nm) [W-H plots]**	**Optical Energy gap, E_g (eV)**
1	30	49	5.38
3	31	53	5.52
5	32	35	5.57
7	30	48	5.64
9	31	58	5.70
11	30	65	5.80

Table.3: J-O intensity parameters (Ω_2, Ω_4), Emission peak wavelengths (λ_p in nm), radiative transition probability (A_T), calculated radiative lifetime (τ_{rad}) and branching ratio (β_R) of $YAlO_3$: Nd^{3+} compounds (λ_{ex} = 364 nm).

Nd^{3+} conc. (mol%)	**J-O intensity parameters($\times10^{-20}$ cm^2)**		**Emission peak wavelength λ_p in nm**	**A_T (s^{-1})**	**τ_{rad} (ms)**	**β_R**
	Ω_2	**Ω_4**				
1	2.87	5.01	596.98	52.18	19.16	0.99
3	3.27	7.76	597.01	59.46	16.81	0.99
5	3.13	6.92	597.01	56.89	17.57	0.99
7	3.10	6.77	596	56.42	17.72	0.99
9	3.37	8.01	597.01	61.35	16.29	0.99
11	3.49	8.34	596	63.43	15.76	0.99

Table 4: The values of CIE (x, y) coordinates and CCT (K) of $YAlO_3$: Nd^{3+} (1-11mol %) NPs.

Nd^{3+} Concentration (mol %)	**X**	**Y**	**CCT (K)**
1	0.1867	0.2585	6178
3	0.1819	0.2502	6177
5	0.1820	0.2514	6176
7	0.1900	0.2719	6180
9	0.1904	0.2738	6174
11	0.1866	0.2665	6172

Table 5: Different nanomaterials used for develop FPs by different authors.

SI. No	Sample	Synthesis technique	Emission Color	References
1	$NaYF_4$:Yb,Er	Solvothermal method	Green	Meng Wang et al. [36]
2	NaYF4:Yb,Er/Ce	Hydrothermal method	Green	Han-Han Xie et al.[37]
3	$Sr_4Al_{14}O_{25}$: Eu^{2+},Dy^{3+}	Combustion method	Blue–Green shade	Vishal Sharma et al.[38]
4	ZnO	Solvothermal method	Green	Mi Jung Choi et al[39]
5	CdSe	Hydrothermal method	Blue	Yuan Feng Wang et al [40]
6	Eu^{3+}:$Y_2Ti_2O_7$ / SiO_2	Sol–gel method	Red	M. Saif et al [41]
7	Eu^{3+} :$Y_2Zr_2O_7$/SiO_2	Sol–gel method	Red	M. Saif [11]

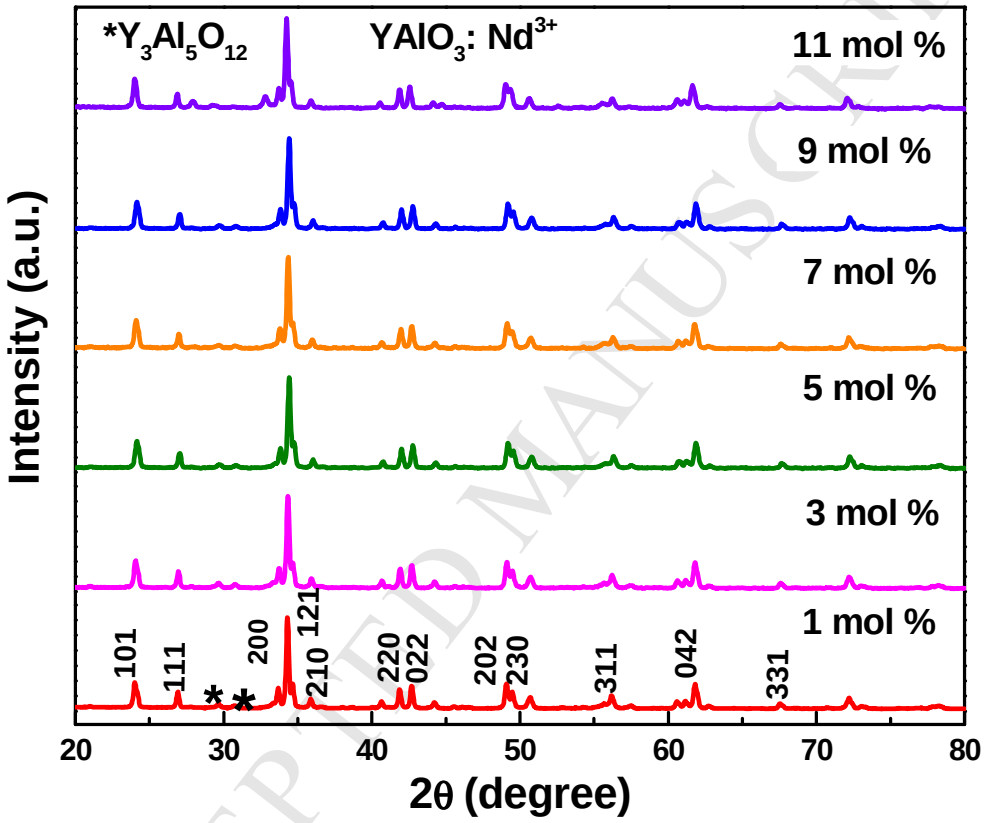

Fig.1. PXRD patterns of (1–11 mol %) Nd^{3+} doped $YAlO_3$NPs.

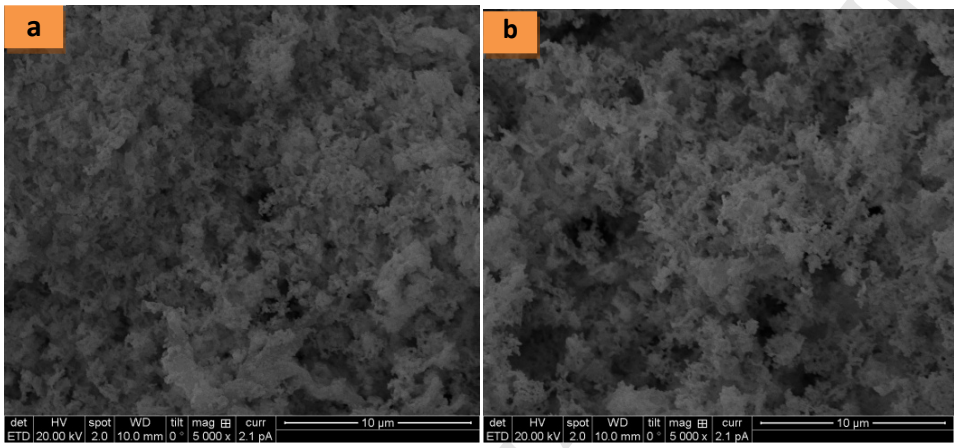

Fig. 2(a-b).SEM micrographs of $YAlO_3:Nd^{3+}$ (3 and11 mol %) NPs.

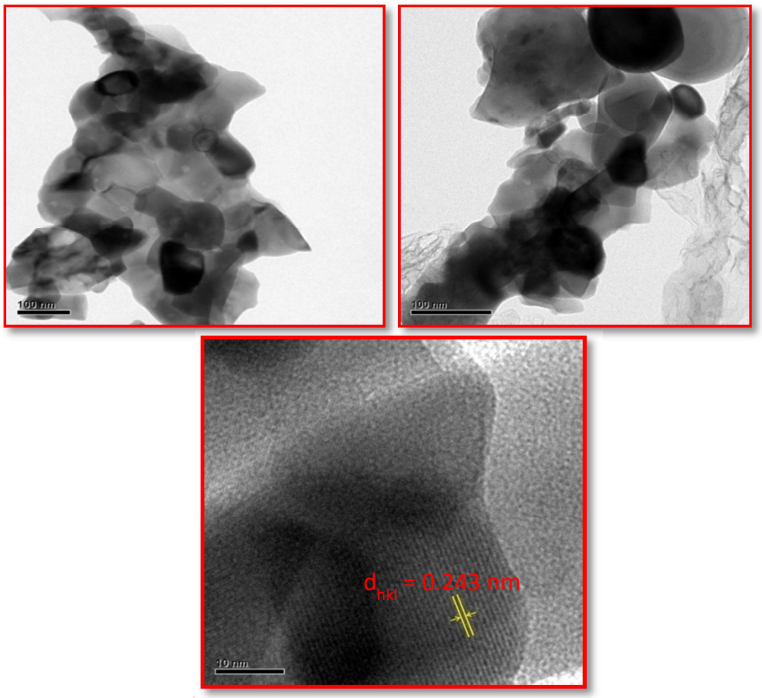

Fig. 3(a-b).TEM micrographs of $YAlO_3:Nd^{3+}$ (3 and11 mol %) NPs, (c) HRTEM image of $YAlO_3:Nd^{3+}$ (5mol %)

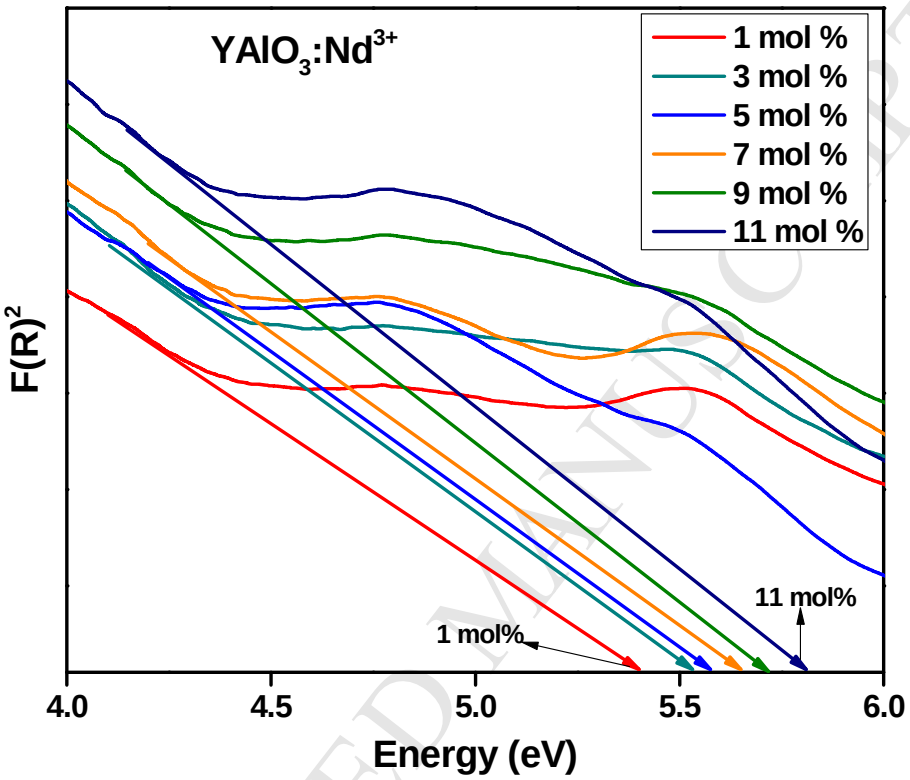

Fig.4.Energy band gaps of Nd^{3+}(1–11 mol %) doped $YAlO_3$NPs.

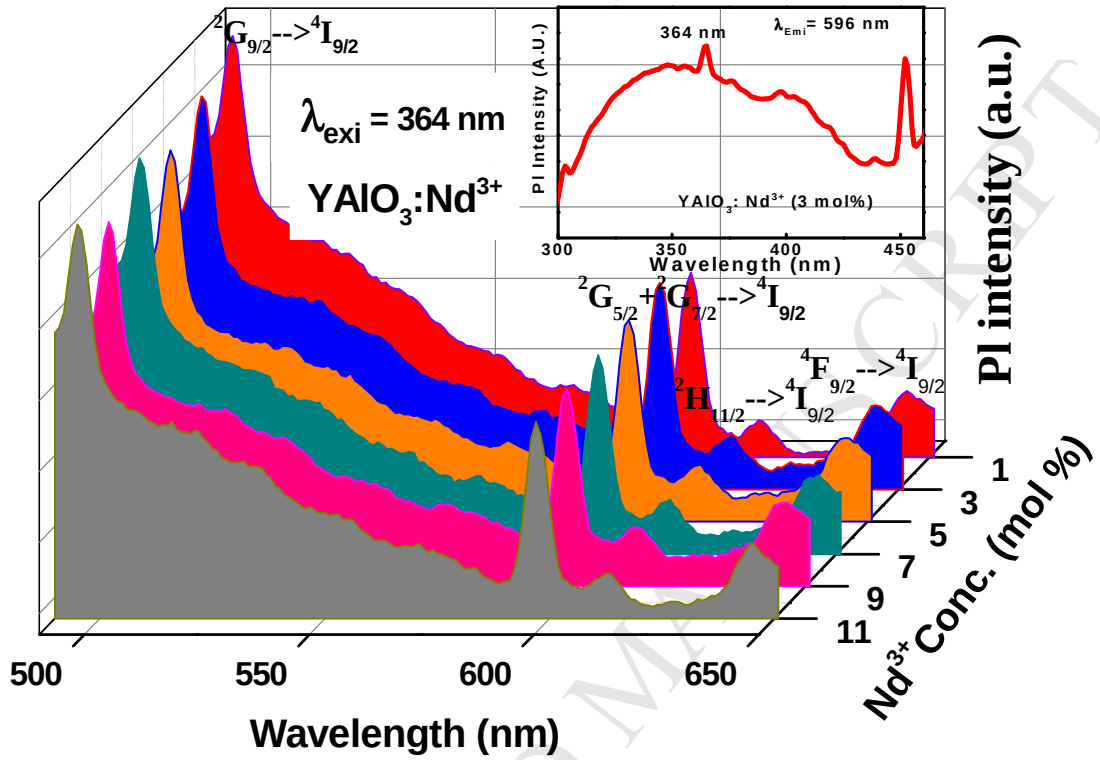

Fig.5. Emission spectrum of $YAlO_3:Nd^{3+}$ (1-11mol %) at λ_{exc}= 364 nm. Inset PL excitation spectra of $YAlO_3:Nd^{3+}$ (3mol %) NPs recorded at RT.

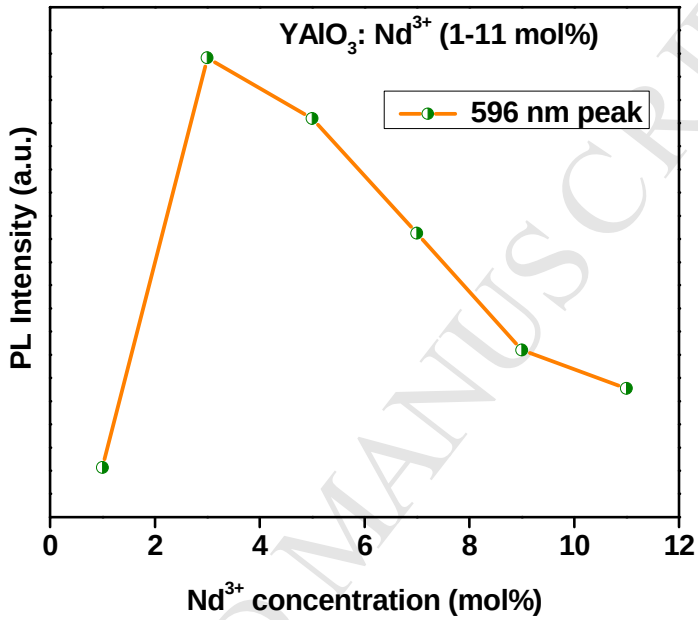

Fig.6. Effect of Nd^{3+}concentration on the 596 nm emission peaks in $YAlO_3$NPs.

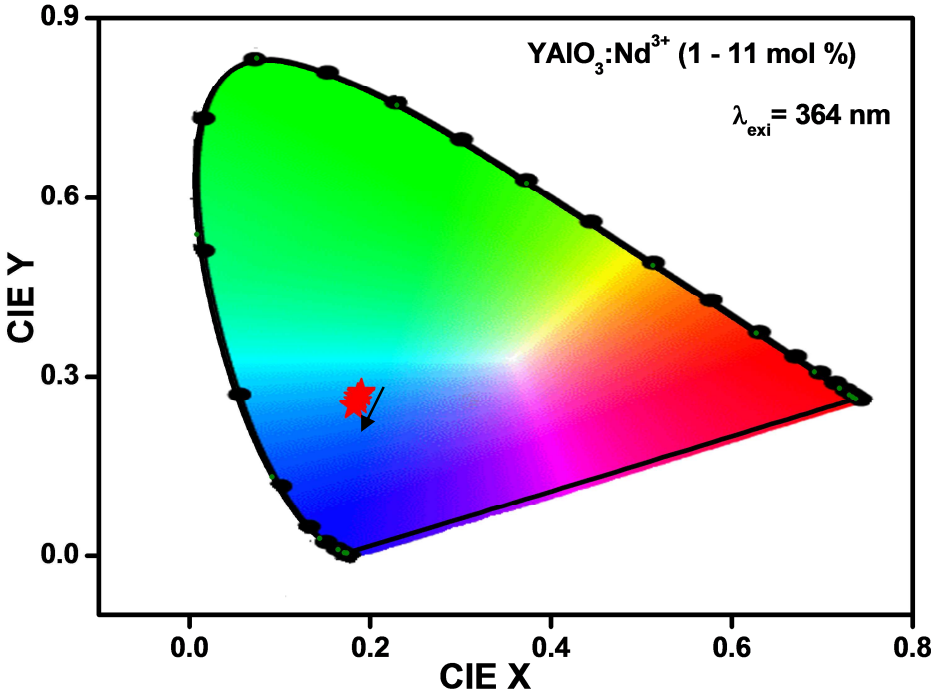

Fig.7. CIE diagram of $YAlO_3:Nd^{3+}$ (1-11 mol %) NPs.

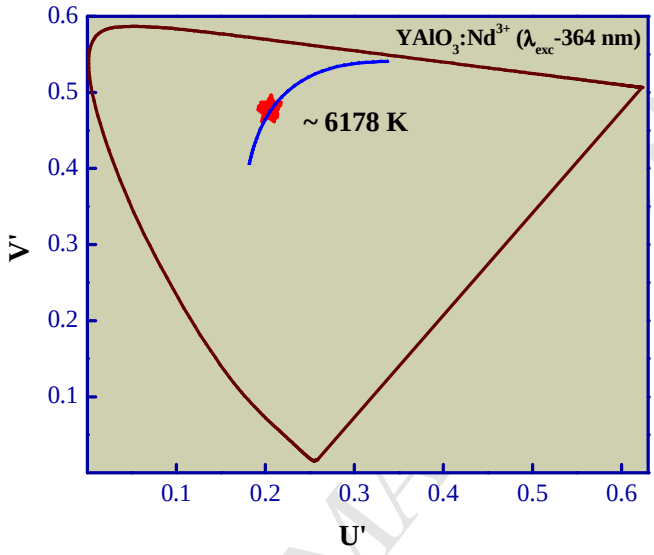

Fig.8. CCT diagram of optimized $YAlO_3$: Nd^{3+} @ 3 mol %

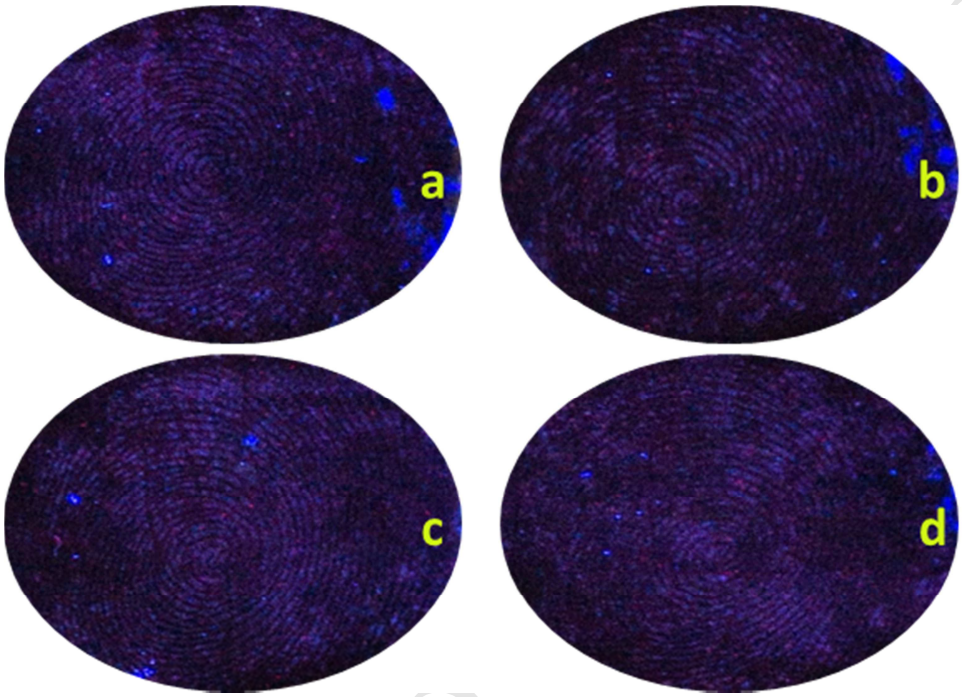

Fig.9. Latent FPs of different persons stained by $YAlO_3:Nd^{3+}$(3mol%) NPs and imaged on the surface of glass.

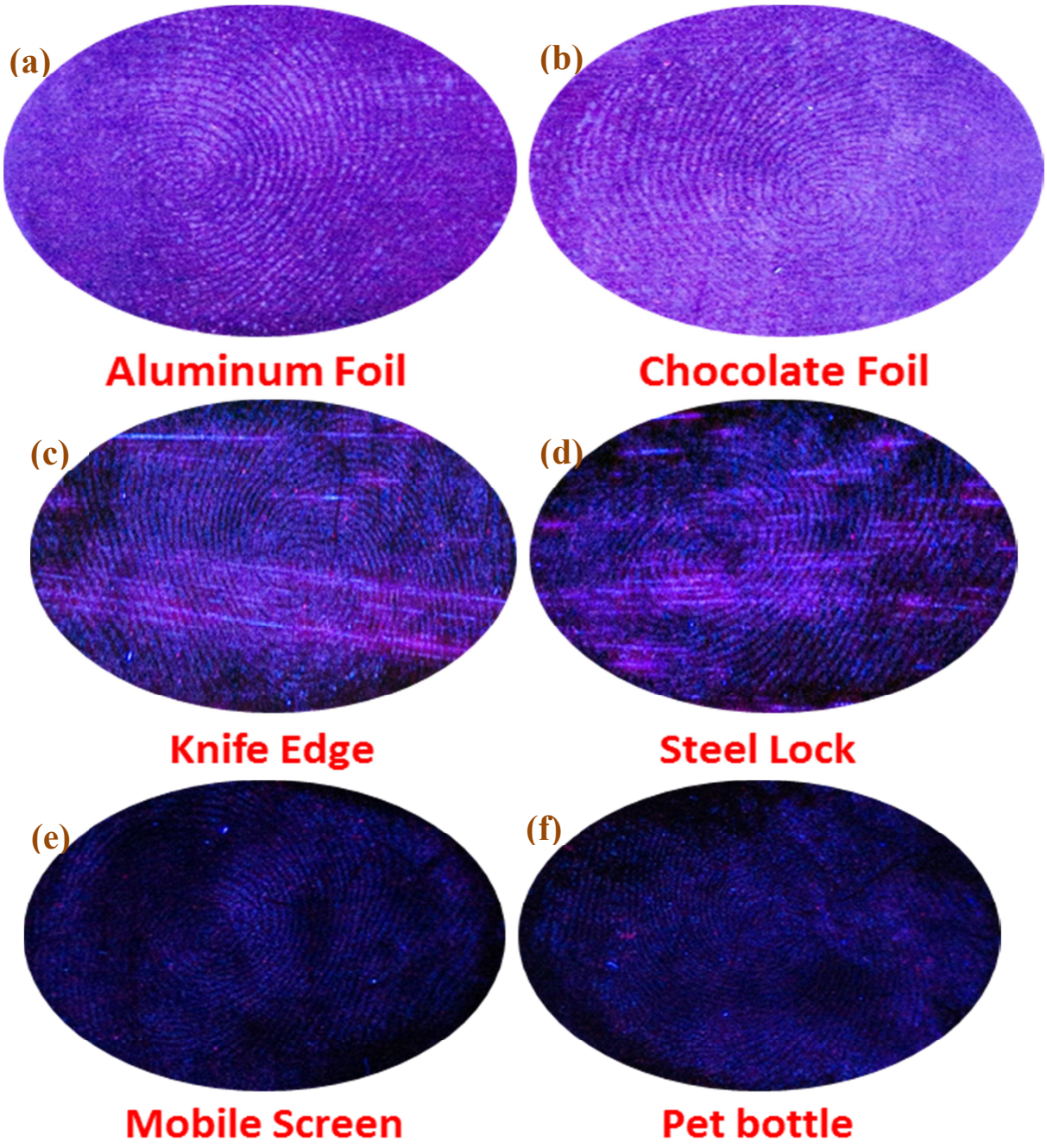

Fig.10.FPs developed by$YAlO_3:Nd^{3+}$(3mol%) NP photographed under 365 nm UV light on an (a) aluminum foil (b) Chocolate wrapping foil (c) surface of knife handle (d) steel lock (e) mobile phone display screen and (f) surface of a PET bottle.

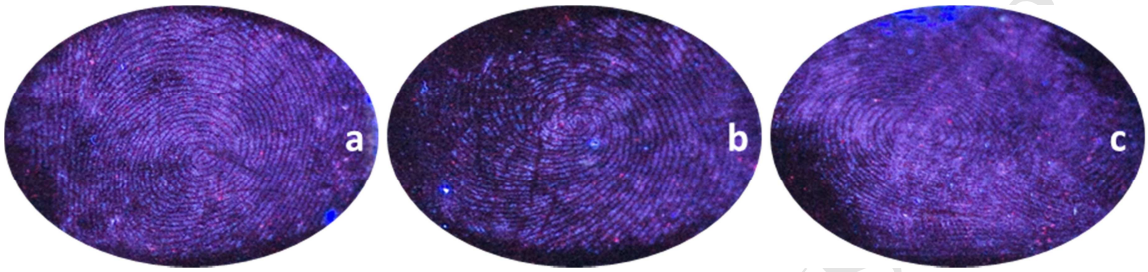

Fig.11. Latent FPs aged on the surface of glass for various periods of time, stained by $YAlO_3:Nd^{3+}$ (3 mol%) and finally detected by 365 nm UV light irradiation (a)1 day, (b) 10 days, (c) 30 days.

Research Highlights:

- $YAlO_3:Nd^{3+}$ nanopowders were used for the rapid visualization of latent fingerprint.
- Average crystallite size is found to be in the range 30 - 32 nm from both TEM & PXRD.
- Blue emission nanophosphor powder material with CCT on the Planckian locus.
- Prepared materials showed better adherence on porous/nonporous and multicolored surfaces.